Deformable microswimmer in an external force field

Mohd Suhail Rizvi, Philippe Peyla, Alexander Farutin, Chaouqi Misbah

Deformable microswimmer in external force field

Mohd Suhail Rizvi,[1,*] Philippe Peyla,[1,†] Alexander Farutin,[1,‡] and Chaouqi Misbah[1,§]

[1] *Laboratoire Interdisciplinaire de Physique, Université Grenoble Alpes and CNRS, F-38000 Grenoble, France*

(Dated: December 18, 2020)

External forces, such as gravity, play significant role in the swimming properties of autonomous biological microswimmers as well as artificial swimming robots. Here we have studied the influence of the external forces on the transport characteristics of the triangular bead-spring microswimmers. The microswimmer, formed by connecting three beads using three springs in an equilateral triangular arrangement, is capable of performing autonomous translational ("mover") and rotational ("rotor") motions. We show that for a mover triangle the application of a small external force results in the alignment of swimming direction with that of the external force, a phenomenon known as 'gravitaxis'. We demonstrate that this gravitactic nature of the active triangle is purely due to the hydrodynamic interaction among the beads. Under large external force, however, the gravitactic nature is lost. This transition from gravitactic to non-gravitactic motion of the microswimmer is characterized by a saddle node or pitchfork bifurcation where the strength of the critical external force scales linearly with the active force amplitude, $f_e^c \sim f_a$. However, for the rotor triangle only saddle node bifurcation is observed which results in a vanishing angular velocity as the strength of the external force is increased. The critical value of the external force for the rotor, however, scales as $f_e^c \sim f_a^{2/3}$. These findings will provide insights into the the nature of biological swimming under gravity, especially the gravitactic microorganisms such as *Chlamydomonas*, as well as guiding the design of under water vehicles.

* mohd-suhail.rizvi@univ-grenoble-alpes.fr
† philippe.peyla@univ-grenoble-alpes.fr
‡ alexandr.farutin@univ-grenoble-alpes.fr
§ chaouqi.misbah@univ-grenoble-alpes.fr

I. INTRODUCTION

Swimming based on a change of shape is deployed by several biological systems [1–4] as well as artificial microswimmers [5–9]. For these microorganisms inertia is negligible and their propulsion is governed by purely viscous forces. In real life biological as well as artificial microswimmers are rarely in isolated environments, and rather often experience external flows and/or forces. Therefore, the presence of external forces, such as gravity in the case of biological organisms or electromagnetic forces for some artificial microswimmers [10, 11], warrants the understanding of their influence on the swimming properties [12].

It is known, for example, that the swimming direction of several biological organisms is influenced by the presence of gravity, a phenomenon known as 'gravitaxis' [13–15]. Among the biological microswimmers, the phenomenon of gravitaxis has been most extensively studied for *Chlamydomonas reinhardtii* [16], a unicellular alga, and *Euglena gracilis* [17], a microscopic protozoan, both of which are found primarily in the fresh stagnant water bodies. These microorganisms utilize cyclic deformations of flagella or the cell body itself to generate propulsion. The proposed mechanisms for the gravitactic motions involve either a biological gravity sensor in the microorganisms [18, 19], or a finite separation between the center of gravity and center of buoyancy (back-heaviness) [16], or the asymmetric shape of the microswimmer [15, 20]. More recently, the behaviors of active colloidal particles [20], Janus particles [21] and squirmers [22, 23] in the presence of external forces have also been the subject of intensive investigations revealing shape asymmetry and collective effects as the possible sources of gravitaxis in these systems. Despite the rich behavior revealed by these rigid microswimmers in the presence of external force, a little is known on the swimmers performing shape change for locomotion.

Here, we consider a triangular bead-spring microswimmer as a prototypical model for swimming thanks to shape change, and analyze the influence of external forces. This type of microswimmer is capable of performing steering motion [8] and have also been used as a model for the swimming of *C. reinhardtii* [24], and magnetocapillary swimmers [10]. This triangular bead-spring microswimmer is a generalization of the linear three-bead microswimmer which moves only along a straight line [7]. The choice of bead-spring microswimmer as a model offers two advantages. Firstly, it would provide a clear understanding of the microswimmer behavior under external forces, and secondly it will allow to shed some new light on the effect of activity on the sedimentation properties of beads [25, 26] and bead-spring assemblies [27, 28]. The sedimentation of a collection of particles has been quite an active area of research since very long time [29, 30]. More recently, the dynamics of the sedimentation of bead assemblies have been studied using analytical and numerical approaches [27, 28, 31, 32], revealing various dynamical behaviors of the passive particles including steady sedimentation [28], hydrodynamic reorientation of asymmetric particles [33], oscillatory solutions [27] as well as chaotic trajectories [34]. In particular, studies on the sedimentation of triplet of beads have shown their sedimentation in a V-shaped stable arrangement [33] or oscillatory solution in the presence of periodic boundary conditions [26]. On the other hand, for the sedimentation of elastic bead-spring assemblies, most of the studies have focused on the dumbbells which demonstrate steady configurations [31] even at finite Reynolds number [28] and oscillatory behaviors which depends on the ratio of gravitational and elastic forces [27]. The present work focuses on the sedimentation of elastic triangular arrangement of the beads in the presence of activity. Besides revealing a rich phase diagram of the microswimmer, this will provide some preliminary results that should help elucidating the influence of activity on sedimentation properties of particle assemblies.

II. TRIANGULAR BEAD-SPRING ASSEMBLY

A. Passive bead-spring triangle

Three identical beads of radii a form an equilateral triangle (Fig. 1) with the help of three springs (equilibrium lengths l, $l \gg a$). This bead-spring assembly is suspended in a fluid of viscosity η and an external force field which exerts force $\mathbf{f}_e$ on each bead. The configuration of the triangle is described by θ, the angle formed between the line joining one of the beads (labeled as bead-1) to the triangle center and the external force direction (Fig. 1). The springs are assumed not to experience the external force or disturb the flow of the surrounding fluid. The triangle although kept in a three-dimensional medium is constrained to move in its plane which contains the direction of the external force.

Under the assumption of negligible inertia of the beads, that is Reynolds number $R_e = 0$, the positions of the three beads satisfy the following equations

$$\frac{d\mathbf{r}_i}{dt} = \mu \mathbf{f}_i\left(\mathbf{r}, t\right) + \sum_{j \neq i} \mathcal{G}_{ij} \cdot \mathbf{f}_j\left(\mathbf{r}, t\right) \tag{1}$$

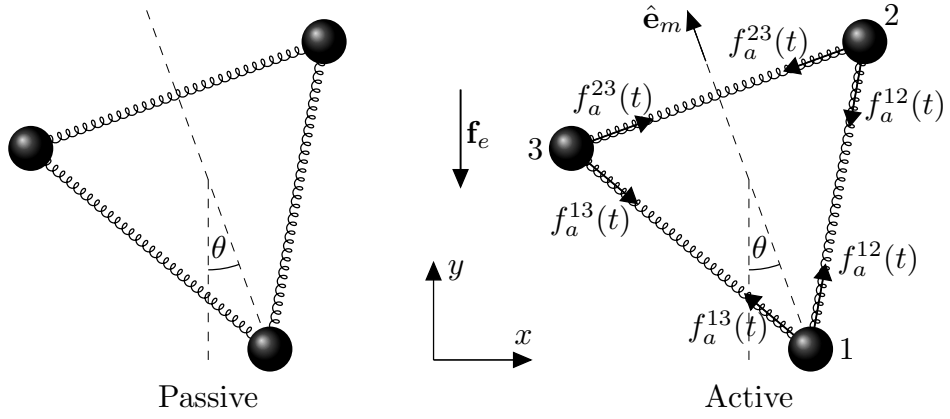

FIG. 1. Schematic of passive (left) and active (right) triangular bead-spring assemblies placed in an external force field $\mathbf{f}_e$. The swimmer orientation θ is characterized by the angle made by the vector joining the triangle center with one of the beads and the direction of external force $\mathbf{f}_e$. The unit vector $\hat{\mathbf{e}}_m$ marks the direction of motion for a mover triangle.

where $\mu = 1/(6\pi\eta a)$ is the mobility of each bead, $\mathbf{f}_i = \mathbf{f}_e + \sum_{j\neq i} \mathbf{f}_s^{ij}$ is the total force (external force + spring force) acting on the ith bead and

$$\mathcal{G}_{ij} = \frac{1}{8\pi\eta}\left(\frac{\mathbf{I}}{r_{ij}} + \frac{\mathbf{r}_{ij}\otimes\mathbf{r}_{ij}}{r_{ij}^3}\right) \tag{2}$$

is the Oseen tensor between the i^{th} and j^{th} beads, and $\mathbf{r}_{ij}$ is the vector joining the i^{th} and j^{th} beads with $r_{ij} = |\mathbf{r}_{ij}|$. It has to be noted that for Oseen tensor to be a valid representation for the hydrodynamic interaction among the beads it requires $l/a \gg 1$. When this condition is not satisfied one can take the bead radii into account by considering Rotne-Prager-Yamakawa tensor [35]. The Oseen tensor corresponds to the velocity field created by a localized force in the Stokes flow

$$\nabla\cdot\mathbf{u} = 0, \quad \eta\nabla^2\mathbf{u}(\mathbf{r},t) - \nabla P(\mathbf{r},t) + \mathbf{f}_p\delta(\mathbf{r}-\mathbf{r}_0,t) = 0 \tag{3}$$

where $\mathbf{u}$ and P are the fluid velocity and pressure, respectively, and $\mathbf{f}_p\delta(\mathbf{r}-\mathbf{r}_0,t)$ is the localized point force at $\mathbf{r}_0$. Here we consider the connecting springs to be finitely extensible nonlinearly elastic (FENE) in nature with resistance force given by

$$f_s^{ij} = -k\frac{\epsilon_{ij}}{1-(\epsilon_{ij}/\epsilon_m)^2} \tag{4}$$

where $\epsilon_{ij} = (r_{ij}-l)/l$ is the spring strain connecting the ith and jth beads, and ϵ_m is the magnitude of the maximum possible strain for the spring. For very small deformations $\epsilon_{ij} \ll 1$ the FENE spring behaves as a linear spring with an elastic constant k.

B. Active bead-spring triangle

In the absence of any external forcing, the above described triangular bead-spring assembly undergoes self-propulsion when periodic active forces (see Fig. 1)

$$f_a^{ij}(t) = f_a^{ij}\sin(\omega t + \alpha_{ij}) \tag{5}$$

are applied on the beads i and j along the connecting springs [8]. This arrangement of active force results in autonomous motion as the total force and torque on the triangle vanish. In general, this active triangle is capable of moving along arbitrary trajectories by appropriately modulating f_a^{ij} and α_{ij} [8]. In this paper, however, we limit ourselves to two specific cases of the active triangle- (i) purely translational motion ("mover") and (ii) purely rotational motion ("rotor"). We can study the swimming behavior of this active triangle using Eq. (1) with $\mathbf{f}_i = \sum_{j\neq i}(\mathbf{f}_s^{ij} + \mathbf{f}_a^{ij})$

as the total force on ith bead. For small force amplitudes $f_a^{ij} \ll k$, we can perform a Taylor series expansion of Eq. (1) in $\boldsymbol{\xi}_{ij}$, the displacement of the ith bead relative to that of the jth bead (see Appendix for details). For equal force amplitudes, that is $f_a^{ij} = f_a \ll k$, and $\alpha_{12} = \alpha_{13} = 0, \alpha_{23} = \alpha$ the triangle moves along a straight line with an average velocity [8]

$$\mathbf{v}_a \approx \sqrt{3}\frac{f_a^2}{kl\eta}\left(\frac{(1-\cos\alpha)+(9\lambda+2/\lambda)\sin\alpha}{16\pi\,(9\lambda+4/\lambda)\,(9\lambda+1/\lambda)}\right)\hat{\mathbf{e}}_m + \mathcal{O}(\xi_{ij}^3) \tag{6}$$

where $\lambda = k\mu/l\omega$ is the ratio of the time scales of the active force actuation $(1/\omega)$ and the triangle deformation $(l/k\mu)$. It needs to be pointed out here that even though the fluid surrounding the swimmer follows Stokes equations (Eq. (3), which are linear) the leading order dependence of swimmer translational velocity (the same holds for the angular velocity, see below) on active force amplitude is quadratic. This non-linear relationship is due to the deformation dependent propulsion mechanism of the swimmer. As in the Stokes problem, the swimmer velocity is proportional to the force amplitude. However, motion takes place only because of the spring deformation, which is proportional to force, hence a quadratic dependence of swimming speed on the force amplitude. This result has to be contrasted with the force-dipole based rigid microswimmer models where the leading order dependence of swimmer velocity on active force amplitude is linear (for an example, see [**?**]). Further, microswimmers are usually classified as 'puller' (e.g. *C. reinhardtii*) or 'pusher' (e.g. *E. coli*) depending on the flow field they generate in the surrounding fluid [1]. This puller-pusher characterization is based on the force-dipole (also known as stresslet Σ) representation of the microswimmer where positive and negative values of stresslet correspond to pusher and puller swimmers, respectively. As reported in [8], for $f_a \ll k$ the mover triangle behaves as a neutral swimmer since the average stresslet over one swimming stroke remains zero. However, for large active force amplitude this ceases to be the case with stresslet $\Sigma \sim \sin\alpha$ which results in puller and pusher like behaviors of the triangle for $\alpha < 0$ and $\alpha > 0$, respectively.

Similarly, for $f_{ij} = f_a \ll k$ and $\alpha_{12} = \mp 2\pi/3, \alpha_{23} = 0$, and $\alpha_{13} = \pm 2\pi/3$ the triangle performs pure rotational motion with an angular velocity

$$\Omega_a = \pm 9\frac{\mu f_a^2}{kl}\frac{1}{9\lambda+4/\lambda} + \mathcal{O}(\xi_{ij}^3). \tag{7}$$

where negative and positive signs correspond to the clockwise and anti-clockwise rotations of the triangle in its plane, respectively. The swimming behavior of the active triangle in the presence of external force can be studied by solving Eq. (1) with

$$\mathbf{f}_i = \mathbf{f}_e^i + \sum_{j\neq i}\left(\mathbf{f}_s^{ij} + \mathbf{f}_a^{ij}\right) \tag{8}$$

where the three terms on right hand side correspond to external force, spring force and active force on the ith bead. In the following we study the behavior of passive and active triangle in the presence of external force analytically as well as numerically. In the analytical treatment we consider small deformation of the triangle (see details below) and validate the obtained expressions by numerical simulation of the Eq. 1 with Eqs. (2), (4) and (8). For the numerical simulations we utilized the `odeint` function of the `scipy` library in `Python`.

III. RESULTS

A. Passive bead-spring triangle

In order to delineate the effect of the interaction between the triangle activity and the external force field we first need to understand the sedimentation properties of a passive triangle ($f_a^{ij} = 0$). In the absence of any hydrodynamic interaction among the three beads, the passive triangle remains undeformed and undergoes purely translational motion with a constant velocity $\mu\mathbf{f}_e$. Hydrodynamic interactions among the beads result in the triangle deformation and rotation. For small deformations of the triangle, Eq. (1) can be linearized to obtain the angular velocity of rotation

$$\dot{\theta} = \Omega_e \approx -Bf_e^3\sin(3\theta) + \mathcal{O}(\xi_{ij}^4) \tag{9}$$

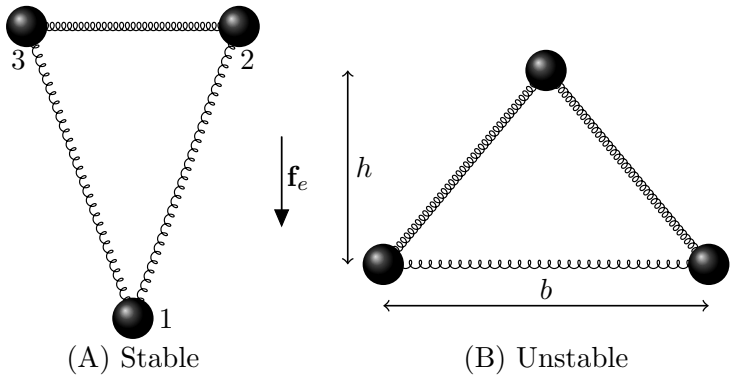

FIG. 2. Schematics of (A) stable and (B) unstable steady state configurations of a passive triangle in an external force field $\mathbf{f}_e$.

where $B = \dfrac{15\sqrt{3}}{512\pi}\left(\dfrac{a^2}{\eta l^4 k^2}\right) > 0$. Further, the translational velocity of the passive triangle $\mathbf{v}_e$, described by the components in the directions normal (but within the plane of triangle) and parallel to the external force

$$v_e^{\perp} \approx \frac{\sqrt{3}a}{64\pi\eta l^2}\frac{f_e^2}{k}\sin(3\theta) + \mathcal{O}(\xi_{ij}^3) \tag{10}$$

$$v_e^{\parallel} \approx \mu f_e + \frac{3f_e}{8\pi\eta l}\left(1 - \frac{a}{16l}\right) + \frac{\sqrt{3}af_e^2}{64\pi\eta l^2 k}\cos(3\theta) + \mathcal{O}(\xi_{ij}^3), \tag{11}$$

respectively, depends on its orientation θ. The first two terms in the expression for $v_e^{\parallel}$ (Eq. (11)) correspond to the sedimentation velocity of a rigid bead-spring triangle whereas the last term in the Eq. (11) and velocity component $v_e^{\perp}$ (Eq. (10)) are due to the triangle deformability. For a rigid equilateral triangle there is no transverse migration owing to its symmetry. This may not be true for a rigid irregular triangular arrangement of beads. The f_e^2 term in Eq. (10) reflects the combination of the deformation (proportional to f_e) and the forces on the beads which are also proportional to f_e. This explains the result in Eq. (9), which is the product of velocity (proportional to f_e^2) and deformation (proportional to f_e). The 3θ dependence of Ω_e and $\mathbf{v}_e$ are the direct consequence of the equilateral triangular shape of the assembly. For a triangle of asymmetric shape (for example, isosceles) we expect this dependence to change from 3θ to θ as seen in biological as well artificial gravitactic microswimmers [15, 20].

The expression for Ω_e (Eq. (9)) shows that there exist one stable (corresponding to $\theta = 0, 2\pi/3$ and $4\pi/3$) and one unstable (corresponding to $\theta = \pi/3, \pi$ and $5\pi/3$) steady state configurations of the passive triangle relative to the external force (Fig. 2). In the stable steady state configuration, the triangle gets elongated along the direction of external force whereas in the unstable configuration it is stretched in the direction normal to the external force field. These two steady state configurations can be described by

$$h \approx \frac{\sqrt{3}l}{2} \pm \frac{3f_e}{8k}a + \mathcal{O}(\xi_{ij}^2), \tag{12}$$

$$b \approx l \mp \frac{\sqrt{3}f_e}{4k}a + \mathcal{O}(\xi_{ij}^2) \tag{13}$$

as the heights and base lengths of the isosceles triangle, respectively. It can be seen that in order to keep the linearization of Eq. (1) valid, we must have, according to the above expressions, $\dfrac{f_e}{k} \ll \dfrac{4l}{\sqrt{3}a}$.

Further, elimination of $\sin(3\theta)$ from equations (9) and (10) shows that $v_e^{\perp}$ is proportional to $\dot{\theta}$. This demonstrates that in the steady state configuration ($\dot{\theta} = 0$, Fig. 2A) the lateral motion of the passive triangle ceases. In the following we will analyze the impact of activity of the mover and rotor triangles on their behavior under the action of external force fields.

B. Active bead-spring triangle

In order to analyze the effect of activity on the triangle dynamics in the presence of external forces, we calculate the average translational and angular velocities over one cycle of the active force. In the following, we describe the

behavior of mover and rotor triangles.

1. Translation of a mover in external force field

In the presence of an external force and activity we calculate the translational velocity of the triangular swimmer by averaging Eq. (1) as

$$\mathbf{v}_m = \frac{2\pi}{3\omega}\sum_{i=1}^{3}\int\left(\mu\mathbf{f}_i + \sum_{j\neq i}\mathcal{G}_{ij}\cdot\mathbf{f}_j(t)\right)dt \tag{14}$$

where $\mathbf{f}_i = \mathbf{f}_e^i + \sum_{j\neq i}\left(\mathbf{f}_s^{ij} + \mathbf{f}_a^{ij}\right)$ is total force on the ith bead with contributions from external force, spring force and activity, respectively. On averaging over the active force cycle for all three beads the first term in the above equation has contributions only from the external force. For small triangle deformation, the integrand in the Eq. (14), can be expanded as a Taylor series of the triangle deformation ξ_{ij} (see Appendix for details) to obtain the leading order terms in the expression of sedimentation velocity of a mover triangle ($f_a^{ij} = f_a$, and $\alpha_{12} = \alpha_{13} = 0, \alpha_{23} = \alpha$) as

$$\mathbf{v}_m = \mathbf{v}_e + \mathbf{v}_a + \mathbf{v}_{ae}, \tag{15}$$

which is described by three contributions: $\mathbf{v}_e$, the passive sedimentation velocity due to external force (given by Eqs. (10) and (11)); $\mathbf{v}_a$, the velocity due to the active propulsion (Eq. (6)); and $\mathbf{v}_{ae}$, the effect of the coupling between the active and the external forces with components

$$v_{ae}^{\perp} = v_{ae}\sin(2\theta) \tag{16}$$

$$v_{ae}^{\parallel} = v_{ae}^{0} - v_{ae}\cos(2\theta) \tag{17}$$

where

$$v_{ae}^{0} \approx \frac{3f_e}{16\pi}\left(\frac{\mu f_a^2}{\eta k\omega l^2}\right)\frac{\lambda\left(18\cos\alpha + 63\right) + \left(14\cos\alpha + 22\right)/\lambda}{\left(9\lambda + 4/\lambda\right)\left(9\lambda + 1/\lambda\right)} + \mathcal{O}(\xi_{ij}^4) \tag{18}$$

$$v_{ae} \approx \frac{f_e}{16\pi}\left(\frac{\mu f_a^2}{\eta k\omega l^2}\right)\frac{\left(153\lambda^2 + 19\right)\left(\cos\alpha - 1\right) + 18\sin\alpha}{\left(9\lambda + 4/\lambda\right)\left(9\lambda + 1/\lambda\right)} + \mathcal{O}(\xi_{ij}^4) \tag{19}$$

Due to the sinusoidal nature of the active force it can be seen that the terms proportional to $f_e f_a$ and $f_a f_e^2$ in the Eq. (14) vanish on averaging over one active force cycle.

Equation (18) shows that even for $\alpha = 0$, corresponding to the active triangle but with zero translational and rotational velocities, the sedimentation velocity is enhanced due to its activity.

2. Gravitaxis

Similar to passive triangle, the active mover triangle also demonstrates rotation in the presence of external force. The average angular velocity of the rotation is given by

$$\Omega_m = \Omega_e + \Omega_{ae}. \tag{20}$$

where

$$\begin{aligned}\Omega_{ae} &\approx -\frac{\sqrt{3}}{8\pi}\left(\frac{\mu f_a^2}{\eta k\omega l^3}\right)\left(\frac{\left(27\lambda + 1/\lambda\right)\left(1 - \cos\alpha\right) + 18\sin\alpha}{\left(9\lambda + 4/\lambda\right)\left(9\lambda + 1/\lambda\right)}\right)f_e\sin(\theta) + \mathcal{O}(\xi_{ij}^4)\\ &\approx -Af_a^2 f_e\sin(\theta) + \mathcal{O}(\xi_{ij}^4)\end{aligned} \tag{21}$$

is the rotation due to the coupling between activity and the external forcing. This shows that we can write the equation for the mover triangle orientation as (where we use that $\Omega_m = \dot{\theta}$ in Eq. (20))

$$\dot{\theta} \approx \left[-Af_a^2\sin(\theta) - Bf_e^2\sin(3\theta)\right]f_e + \mathcal{O}(\xi_{ij}^4) \tag{22}$$

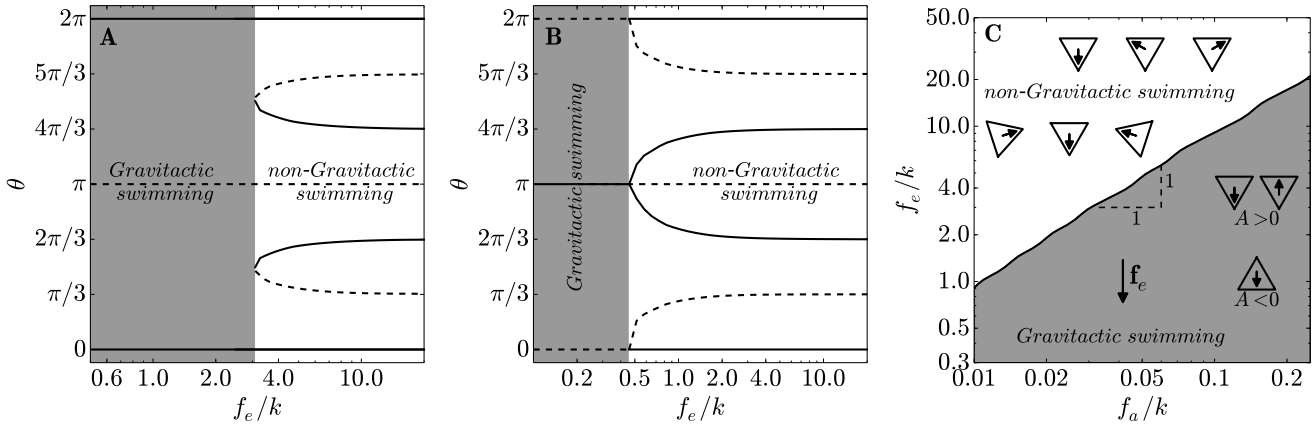

FIG. 3. Bifurcation diagrams for the gravitactic swimming of a mover with (A) $A > 0$ and (B) $A < 0$ as obtained from the numerical simulation of Eq. (1). For $f_e < f_e^c$, the swimming direction for a pusher ($\alpha > 0$) is same as that of external force. For a puller swimmer ($\alpha < 0$), however, the swimming direction depends on the sign of A (also see Fig. 4). The solid and dashed lines represent the stable and unstable steady states, respectively. Values of other parameters are $f_a/k = 0.03$, $l/a = 100$, $\alpha = \pi/2, -\pi/4$, and $\lambda = 0.8$, 0.3. (C) Phase diagram of the mover triangle from the numerical simulation of Eq. (1) for different values of active and external forces. The critical value of the external force separating the gravitactic (shaded region) and non-gravitactic behaviors scales linearly with the active force amplitude. The triangles represent the steady state behavior of the microswimmer in the presence of $\mathbf{f}_e$ with the arrows in the triangles denoting the respective direction of autonomous propulsion.

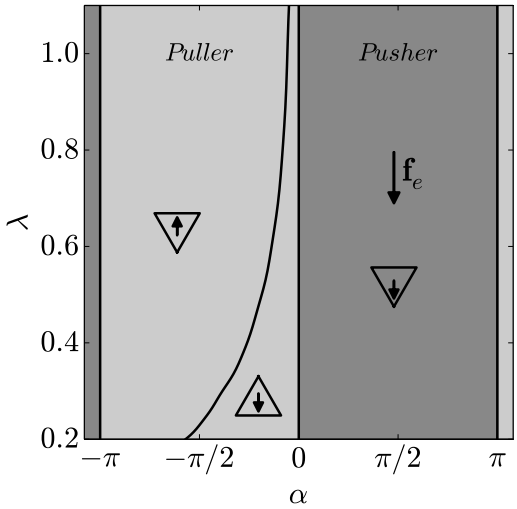

FIG. 4. Phase diagram showing swimming direction of puller ($-\pi < \alpha < 0$) and pusher ($0 < \alpha < \pi$) swimmers in the gravitactic regime as obtained from numerical simulation of the mover triangle. The triangles in the three regions represent the steady state swimmer configuration with the arrows denoting respective swimming directions. Values of other parameters are $l/a = 100$, $f_a/k = 0.01$ and $f_e/k = 0.5$.

where coefficients A and B are given by Eqs. (21) and (9), respectively. It can be seen that for $|A|f_a^2 \gg Bf_e^2$, that is, for large active force as compared to external force, there is only single stable steady state $\theta = 0$ (for $A > 0$) or $\theta = \pi$ (for $A < 0$). In other words, for very weak external forces the triangle aligns its swimming direction with that of the external force field resulting in gravitactic swimming [14, 15] (Fig. 3A-B). This gravitactic behavior of the mover triangle can be understood as follows. In the absence of external force the swimming direction is arbitrary (there is continuous degeneracy, in that any direction is equivalent). Switching on the external force on the mover breaks down the continuous family of directions into a discrete set of solutions $n\pi$, where, for $A > 0$, 0 corresponds to a stable (unstable for $A < 0$) and π to unstable (stable for $A < 0$) solution (modulo 2π). For $|A|f_a^2 \ll Bf_e^2$ the external

force dominates the triangle dynamics resulting in three stable steady states (similar to passive triangle, see Eq. (9)) and the triangle gets trapped in any of these three steady states depending on its initial configuration. Therefore, for strong external forcing the gravitactic nature of the mover triangle is lost. A close inspection of Eq. (22) shows that depending on the values of A, which describes the flagellar beating pattern and frequency, the transition between the gravitactic and non-gravitactic swimming of the mover triangle is described by a saddle node (for $A > 0$, Fig. 3A) or pitch fork (for $A < 0$, Fig. 3B) bifurcation where the critical value of the external force is given by

$$(f_e^c)^2 \approx \chi \frac{A}{B} f_a^2, \tag{23}$$

where $\chi = 1, -1/3$ for $A > 0$ and $A < 0$, respectively. This shows that the critical value of the active force amplitude scales linearly with the external force (Fig. 3B).

Further, it can be seen in Figs. 3A-B that for an external force just beyond f_e^c the triangle orientation corresponding to the stable steady states is not the same as that for the passive triangle (which is equal to 0 and $2\pi/3$ for the stable positions). For $f_e \gg f_e^c$, however, the steady state orientations coincide with those for the passive triangle (Fig. 2).

As mentioned earlier, even though in the gravitactic regime the swimming direction gets aligned with the external force its exact nature ($\theta = 0$ or π), however, depends on A via α and λ. In fact for $f_a \ll k$ in the gravitactic regime for $\alpha \in [\alpha_c, 0]$, where

$$\cos\alpha_c = 1 - \frac{648}{(27\lambda + 1/\lambda)^2 + 324} \text{ and } \alpha_c < 0 \tag{24}$$

the $\theta = \pi$ orientation (which is unstable for passive triangle) becomes stable and $\theta = 0$ becomes unstable. This, combined with the dependence of swimmer propulsion direction on λ and α, results in three distinct swimmer behaviors as shown in Fig. 4. For $\alpha > \alpha_c$ the swimming direction is along the external force direction whereas for $\alpha < \alpha_c$ it is opposite to the external force. Further, for $\lambda \gg 1$, that is very slow swimming strokes relative to the relaxation time of the swimmer, and $f_a \gg k$ we get $\alpha_c \sim 0$. This demonstrates distinct behaviors for puller and pusher swimmers under external force where pullers tend to swim opposite to the external force and pushers along the external force.

3. Rotor in an external force field

We have seen in the last section the effect of external force on the straight trajectory (a mover) of the triangle. Here we consider the other limit where the unperturbed swimmer is a rotor. In the absence of any external force the rotor triangle ($f_{ij} = f_a$, $\alpha_{12} = -\alpha_{13} = \mp 2\pi/3$ and $\alpha_{23} = 0$) performs only rotational motion with an angular velocity Ω_a (Eq. (7)). In the presence of external force the leading order terms in the angular velocity

$$\Omega_r = \Omega_a + \Omega_e + + \mathcal{O}(\xi_{ij}^4) \tag{25}$$

are due to the active rotation and the rotation due to external force, respectively. From the expressions of Ω_e (Eq. (9)) and Ω_a (Eq. (7)), we can write the equation for the orientation of rotor triangle as

$$\dot{\theta} \approx C f_a^2 - B f_e^3 \sin(3\theta) + \mathcal{O}(\xi_{ij}^4) \tag{26}$$

where coefficient C (which can be positive or negative depending on the active force distribution) is easily read off Eq. (7) and $B > 0$ (see Eq. (9)). This demonstrates that for $|C| f_a^2 \gg B f_e^3$ (weak external forcing) the swimmer rotates with nearly a constant angular velocity (shaded region in Fig. 5). On the contrary, for $|C| f_a^2 \ll B f_e^3$ (strong external forcing) the swimmer rotation stops and it gets trapped in one of the three steady states described by Eq. (9). Similar to the mover triangle the qualitative change in the behavior of the rotor triangle as the strength of the external forcing is increased, can be characterized by a saddle node bifurcation (Fig. 5A). Eq. (26) shows that the critical value of the external force at the bifurcation point is given by

$$(f_e^c)^3 \approx \frac{|C|}{B} f_a^2 \tag{27}$$

and it scales with the active force amplitude as $f_e^c \sim f_a^{2/3}$ (Fig. 5B).

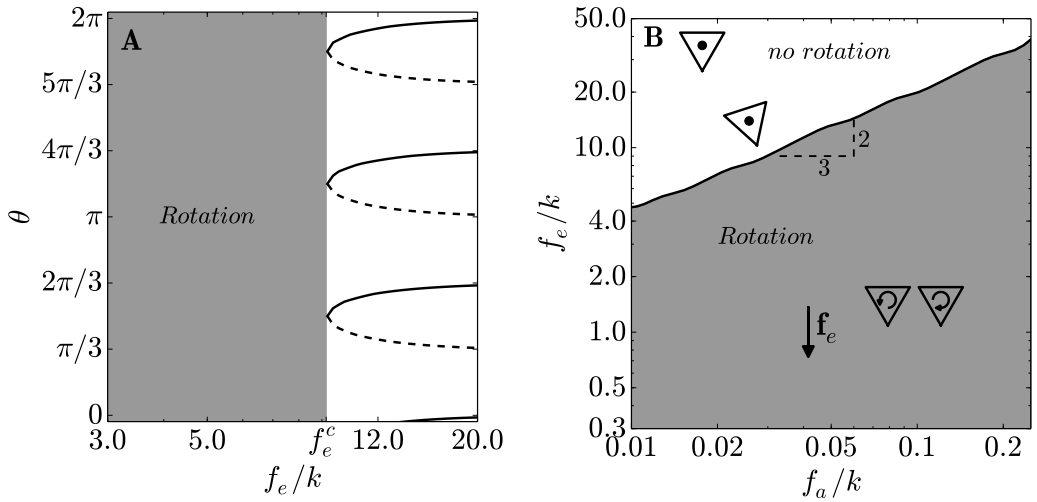

FIG. 5. (A) Bifurcation diagram for the rotor triangle from the numerical simulation of the rotor triangle. For $f_e < f_e^c$, the rotor triangle has a non-zero angular velocity. The solid and dashed lines represent the stable and unstable steady states, respectively. Values of other parameters are $f_a/k = 0.03$, $l/a = 100$, and $\lambda = 0.8$. (B) Phase diagram of the rotor triangle as obtained from numerical simulations. The critical value of the external force separating the rotating (shaded region) and non-rotating states scales as $f_e^c \sim f_a^{2/3}$.

4. Lateral migration of a rotor

Recall that in the absence of any external force the rotor does not show any translational motion. The application of external forcing, however, results in a lateral migration along with an enhancement of mobility along the external force direction. The total velocity for the rotor with $\alpha_{12} = \mp 2\pi/3$, $\alpha_{23} = 0$ and $\alpha_{31} = \pm 2\pi/3$ is given by

$$\mathbf{v}_r = \mathbf{v}_e + \hat{\mathbf{v}}_{ae} \tag{28}$$

where the components of $\hat{\mathbf{v}}_{ae}$ are

$$\hat{v}_{ae}^{\perp} \approx \pm \frac{27 f_e}{768\pi^2} \left(\frac{f_a^2}{k^2 \eta^2 l^2 \mu} \right) \frac{1}{9\lambda + 4/\lambda} + \mathcal{O}(\xi_{ij}^4) \tag{29}$$

$$\hat{v}_{ae}^{\parallel} \approx \frac{27 f_e}{32\pi} \left(\frac{\mu f_a^2}{\eta k \omega l^2} \right) \frac{1}{9\lambda + 4/\lambda} + \mathcal{O}(\xi_{ij}^4) \tag{30}$$

It is noteworthy that the leading order terms in the velocity due to the coupling between activity and external force do not depend on the triangle orientation. Further, the direction of lateral migration ($\hat{v}_{ae}^{\perp}$) depends on the nature of the active forcing. A reversal of the direction of active rotation (by modulation of α_{ij}) also results in the reversal of the direction of lateral migration.

C. Velocity fields

In order to gain further insights into the nature of the swimming of the active triangle in the presence of external force we calculate the velocity fields generated by these microswimmers in the surrounding fluids. For a passive triangle, the steady state fluid velocity in the reference frame attached to the triangle is given by

$$\mathbf{u}_p(\mathbf{r}) = -\mathbf{v}_e + \mathbf{u}_e(\mathbf{r}) + \mathbf{u}_{FD} \tag{31}$$

where $\mathbf{v}_e$ is the velocity of triangle sedimentation, $\mathbf{u}_e(\mathbf{r}) = \sum_{i=1}^{3} \mathcal{G}(\mathbf{r}, \mathbf{r}_i)\, \mathbf{f}_e$ (where $\mathbf{r}_i$ is the position of ith bead and $\mathcal{G}$ is given by Eq. (2)) is the velocity induced by the external force $\mathbf{f}_e$ acting on the beads, and $\mathbf{u}_{FD}(\mathbf{r})$ is the velocity field due to the deformation of the triangle.

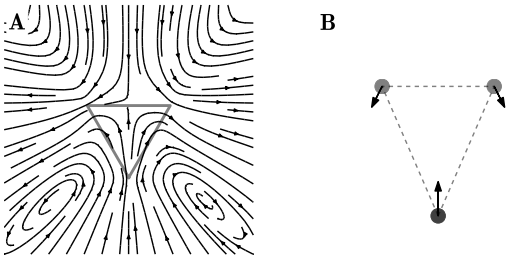

FIG. 6. (A) Velocity field $\mathbf{u}_{FD}$ due to the force-dipoles induced by the passive bead-spring triangle in external force field. Parameter values are $l/a = 100$, $f_e/k = 1$. (B) Schematic showing the forces acting on the three beads of the passive triangle in the reference frame co-moving with the triangle.

Fig. 6A shows the nature of $\mathbf{u}_{FD}(\mathbf{r})$ in the reference frame attached to the passive triangle. It can be seen that this velocity field resembles the one due to the swimming of *Chlamydomonas*, a biflagellated alga [36]. This is expected since in the steady state the passive triangle gets elongated in the direction of the external force which leads to three point forces (or stokeslets) acting on the three beads, which is also a simplified representation of *Chlamydomonas* for the far-field velocity field [36]. In the calculations of the far-field fluid velocity these stokeslets can also be represented as as three force dipoles along the three connecting springs (Fig. 6B). We obtain the leading order terms in the far-field $\mathbf{u}_{FD}$ as

$$\mathbf{u}_{FD}(\mathbf{r}) \approx \frac{9\sqrt{3}a}{128\pi\eta}\frac{f_e\mathbf{r}}{r^5}\left(r^2 - 3\frac{(\mathbf{r}\cdot\mathbf{f}_e)^2}{f_e^2}\right) + \mathcal{O}(\xi_{ij}^2) \tag{32}$$

which shows a $1/r^2$ dependence, as expected from the force-dipoles. This shows that the terms $\mathbf{u}_e$ and $\mathbf{u}_{FD}$ in the Eq. (31) decay as $1/r$ and $1/r^2$, respectively. It has to be noted that the velocity field $\mathbf{u}_{FD}$ is independent of stiffness of the springs, k. It can be understood by the fact that for $f_e \ll k$, the linear nature of spring results in triangle deformation by a magnitude which is proportional to f_e/k. Therefore, force acting at each bead due to the triangle deformation is proportional to $k \times f_e/k = f_e$ which is independent of k.

The application of the activity on the triangle results in additional correction $\mathbf{u}_a$ in the velocity field (Fig. 7). As shown previously in [8], the average far-field velocity field due to the mover triangle in the absence of any external force can be represented by a rotlet-dipole. This rotlet-dipole is composed of two rotlets of opposing polarity placed at the beads-2 and 3 (Fig. 7A'). Similarly, for the rotor triangle the far-field velocity field can be expressed in terms of three rotlet-dipoles (Fig. 7C'). The rotlet-dipole representation of the velocity field due to triangle activity, in both of these instances, demonstrates a $1/r^3$ decay of the fluid velocity. The analytical expressions for the far field velocity fields due to mover and rotor triangles are given in [8].

Therefore, in presence of activity ($f_a \gg f_e$) the near-field velocity field in the fluid is primarily due to the swimmer activity, whereas, the far-field is described by the external force. For a mover triangle with $f_a \gg f_e$ its gravitactic property also ensures a symmetric nature of the total fluid velocity about $\mathbf{f}_e$ in the steady state (Fig. 7B-B'). On the other hand, for $f_a \ll f_e$ (non-gravitactic swimming) the fluid velocity is not necessarily symmetric about $\mathbf{f}_e$ since the propulsion direction of the mover is not always aligned with $\mathbf{f}_e$. Similarly, the velocity field due to a rotor triangle in the presence of external force is also not symmetric (Fig. 7D-D')

IV. DISCUSSION

The sedimentation behavior of the passive flexible triangle presents a picture somewhere in between the two extremes of rigid triangle and an unconnected triplet of particles. The rigid triangle sediments with constant velocity (although higher than that of single isolated bead) and the external force does not have any influence on its orientation. On the other hand, an unconnected bead triplet is known to demonstrate many equilibrium configurations, including 'kissing' (where only one pair of beads touch each other) and 'chain' (where there are at least two touching pairs) configurations [37], as well as oscillatory [25, 27] and chaotic solutions [34]. We have seen that for the flexible triangle, the application of external force results in its deformation to an isosceles triangle (Fig. 2). A rigid isosceles arrangement of beads has been known to reorient itself along the external force [33]. Therefore, it can be seen that the external force deforms the equilateral triangle to an isosceles configuration, which, in turn, gets reoriented to align with the external force.

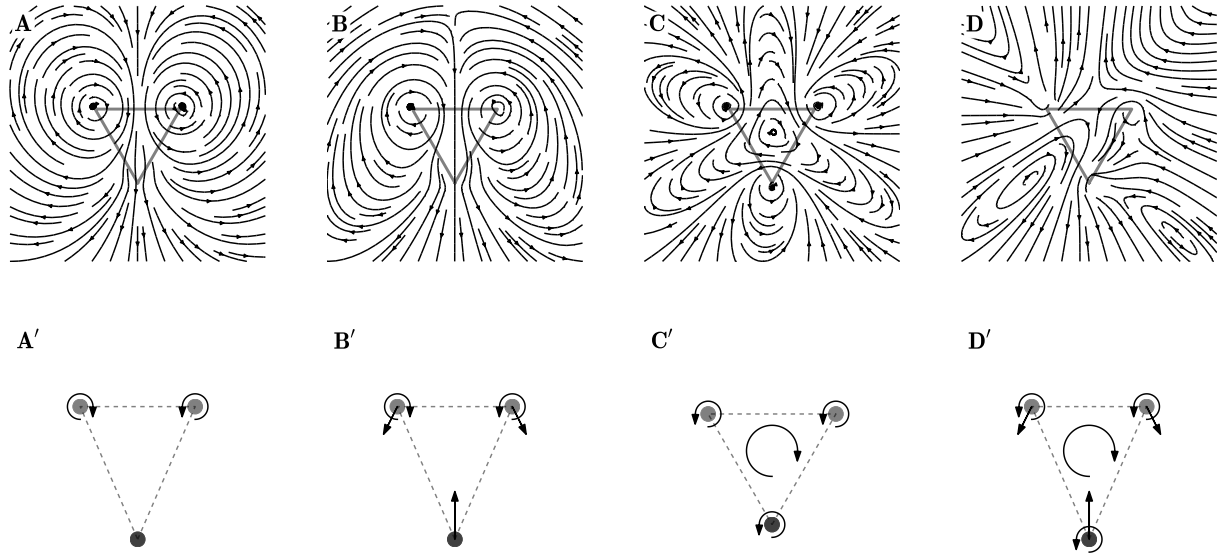

FIG. 7. Velocity fields due to a mover triangle with (A) $f_a/k = 0.01$, $f_e = 0$, (B) $f_a = 0.02$, $f_e = 0.01$, and a rotor triangle with (C) $f_a = 0.01$, $f_e = 0$ and (D) $f_a = 0.02$, $f_e = 0.01$ averaged over one cycle of activity. Other parameters are $l/a = 100$, $\lambda = 0.8$, (A,B) $\alpha_{12} = \alpha_{13} = 0$, $\alpha_{23} = \pi/2$, and (C,D) $\alpha_{12} = -\alpha_{13} = -2\pi/3$, $\alpha_{23} = 0$. Corresponding lower panels show the schematics with the singularity representations where straight and curved arrows mark the average stokeslets and rotlets, respectively.

Although the results shown here are limited to a triangle constrained to move along a vertical plane, it can be easily generalized to a three dimensional bead-spring assemblies such as a tetrahedral arrangement. We do not observe any oscillatory or chaotic regimes for the passive triangle for the range of f_e/k we report in this paper. However, our preliminary results for higher magnitude of external force demonstrate oscillatory as well as chaotic regimes which we hope to report on in the future. The oscillatory solutions of the bead-spring triangle for large external forces can be considered a simplified model of the sedimentation of the deformable and irregular bodies [27, 38]. Furthermore, the oscillatory solutions also raise a possibility of design of passive swimmers under combined force and flow fields [39].

The introduction of the activity further enhances the rich dynamics of the triangle. For the active mover triangle a weak external forcing results in the gravitactic motion. This hydrodynamics based mechanism for the gravitaxis depends on the puller-pusher characteristic. For pullers, such as *C. reinhardtii*, the swimming direction is opposite to the external force (for example gravity). However, pushers, such as *E. coli* and Spermatozoa, swimming in the direction of the external force. Further, considering the case of *C. reinhardtii*, its flagellar beating patterns correspond to $\alpha < 0$ [24]. If we take the following values for the active and external forces $f_a = 0.25k$ and $f_e = 5k$ (values which yield a typical beating pattern) the maximum angular velocity due to the coupling of activity and external force is approximately 0.01-0.05/cycle. This shows that it would take approximately 50-100 cycles for a *C. reinhardtii* to realign its direction for swimming opposite to the gravity. This time is much smaller than the average duration of "free-flight" time (the duration between two consecutive tumbling events) which is close to 10s (or approximately 500-1000cycles) [40]. Furthermore, this hydrodynamics driven gravitaxis also provides more control for the swimming of micro-organisms as opposed to the back-heaviness [16]. As shown in Fig. 4, for hydrodynamic gravitaxis, swimmer can change its direction of swimming, when required, by modulating the beating patterns of the flagella. We also see that by performing an appropriate flagellar beating (such as that for a rotor) a swimmer can undergo rotational motion even in the presence of external forcing. We expect the microorganisms to deploy a combination of 'mover' and 'rotor' states to move along arbitrary trajectories in the presence of the forces such as gravity. Therefore, the hydrodynamics driven gravitaxis shown here offers a new perspective for further experimental investigations which may require micro-gravity setup [41] for gravitaxis. It needs to be highlighted that the deformation of the triangle due to the active or external forces is inversely proportional to the stiffness of the spring k. Therefore, the regimes of high/low external and active forces can also be interpreted as low/high stiffness of the springs. From the analytical expressions it can be seen that the behaviors of active and passive triangles for small external and active forces also correspond to very large values of k.

The reorientation of the swimmer in the presence of external force is also expected to have effects on their behavior in suspensions. The active symmetric rigid particles (movers) have been known to demonstrate polar ordering along the direction of the applied external force [12, 42, 43]. The mechanism of this polar order has been attributed to the rotational diffusion or run-and-tumble nature of the active particles. For the deformable swimmers also, as considered here, we show a polar ordering, albeit in a dilute regime, by virtue of their alignment of swimming direction with that of the external force. However, the mechanism of this polar ordering is of fundamentally different nature since it is caused by its activity driven deformation which does not depend on the rotational diffusion or tumbling of the swimmer. The activity of the mover triangle results in its change of shape from an equilateral triangle to an isosceles one which is known to demonstrate gravitaxis [33]. The properties of collective sedimentation of the triangular active particles would require further systematic analysis.

V. CONCLUSIONS

We have used numerical simulation and analytical approaches to study the behavior of a triangular microswimmer in the presence of external force. We have observed that the flexibility of the connecting springs and the active forces leads to faster movement of the triangle than that of a single particle in the same external force. We have also found that for translational microswimmers an application of weak external force leads to its alignment of propulsion direction with that of external force. Under strong external forces we have shown that there are three distinct stable steady states possible which leads to loss of gravitaxis of translational microswimmer and rotation for rotational microswimmer.

ACKNOWLEDGEMENTS

We thank CNES (Centre National d'Etudes Spatiales) and the French-German University Programme "Living Fluids" (Grant CFDA-Q1-14) for a financial support.

APPENDIX

In the following we provide the details of the derivation of the equations in the main text.

A. Active triangle in the absence of external force

The details of the derivations of the swimming properties of the active triangle in the absence of any external force are given in [8] and [24]. Here, we describe the important steps to obtain Eqs. (6) and (7). The actuation of the active triangle is prescribed by the active forces given by Eq. (5). In the absence of external force ($\mathbf{f}_e = 0$), application of active force results in periodic deformation of the triangle. The average swimming velocity of the triangle in one cycle of the active force can be written as

$$\mathbf{v}_a = \frac{1}{3T}\sum_{i=1}^{3}\int_0^T \left(\mu \mathbf{f}_i\left(\mathbf{r},t\right) + \sum_{j\neq i}\mathcal{G}_{ij}\cdot\mathbf{f}_j\left(\mathbf{r},t\right)\right)dt. \tag{33}$$

where $\mathbf{f}_i = \sum_{j\neq i}(\mathbf{f}_s^{ij} + \mathbf{f}_a^{ij})$ is the total force (spring+active) acting on ith bead and $T = 2\pi/\omega$ is the time period of the active force. The first term on the right hand side of the above equation vanishes due to force free condition $\sum \mathbf{f}_i = 0$. We utilize the Taylor series expansion of the Oseen tensor (Eq. (2)) around the equilibrium triangular configuration to get

$$\mathbf{v}_a = \frac{1}{3T}\sum_{i=1}^{3}\int_0^T \left(\sum_{j\neq i}\left(\boldsymbol{\xi}_{ij}(t)\cdot\nabla\right)\mathcal{G}_{ij}\cdot\mathbf{f}_j\left(\mathbf{r},t\right)\right)dt + \mathcal{O}(\xi_{ij}^3), \tag{34}$$

where $\boldsymbol{\xi}_{ij}(t) = \mathbf{x}_i(t) - \mathbf{x}_j(t)$ represents the small relative displacement of the i^{th} bead with respect to the j^{th} bead (Here $\mathbf{x}_i$ is the displacement of the ith bead from its equilibrium position). Here we have used the force-free condition.

For $|\boldsymbol{\xi}_{ij}| \ll l$, the springs behave linearly and, as a result, we can expand Eq. (1) as a Taylor series to obtain

$$\frac{d\mathbf{x}_i}{dt} = \mu \sum_{j\neq i} \left(f_a^{ij} - \frac{k}{l^2} \boldsymbol{\xi}_{ij} \cdot \mathbf{r}_{ij} \right) \frac{\mathbf{r}_{ij}}{l} + \sum_{j\neq i} \left[\mathcal{G}_{ij}^0 \sum_{m\neq j} \left(f_a^{jm} - \frac{k}{l^2} \boldsymbol{\xi}_{jm} \cdot \mathbf{r}_{jm} \right) \frac{\mathbf{r}_{jm}}{l} \right] + \mathcal{O}(\xi_{ij}^2) \tag{35}$$

where $\mathcal{G}_{ij}^0$ is the Oseen tesor for the undeformed triangle. We can obtain the equation for $\boldsymbol{\xi}_{ij}$ as

$$\frac{d\boldsymbol{\xi}_{ij}}{dt} = \frac{d\mathbf{x}_i}{dt} - \frac{d\mathbf{x}_j}{dt} \tag{36}$$

which is a linear ordinary differential equation in $\boldsymbol{\xi}_{ij}$ with sinusoidal forcing f_a. The general solution to this equation can be written in the form

$$\boldsymbol{\xi}_{ij} = \mathbf{A}_{ij} \sin(\omega t) + \mathbf{B}_{ij} \cos(\omega t) \tag{37}$$

which can be substituted into Eq. (36) to solve for the coefficients $\mathbf{A}_{ij}$ and $\mathbf{B}_{ij}$. This gives a linear dependence of $\boldsymbol{\xi}_{ij}$ on f_a. Therefore, it can be seen from Eq.(34) that the leading order dependence of swimming speed on f_a is quadratic since the terms linear in f_a vanish when averaged over one cycle. In the same spirit the average angular velocity can be written as

$$\Omega_a = \frac{1}{Tl^2} \sum_{i=1}^{3} \mathbf{r}_{ic}^0 \times \int_0^T \mathbf{v}_{ic}(t) dt + \mathcal{O}(\xi_{ij}^3). \tag{38}$$

where $\mathbf{r}_{ic}^0$ is the position vector of the i^{th} bead relative to triangle center of mass and $\mathbf{v}_{ic}(t)$ is the relative velocity of that bead with respect to the center of mass of the microswimmer.
For sufficiently small amplitudes of the active forces, that is $f_a \ll k$, the evolution equations of the beads positions can be obtained up to linear order accuracy ($\mathcal{O}(\boldsymbol{\xi}_{ij})$) from Eq. (1). Substitution of these values of beads position into Eqs. (34) and (38) gives us the translational and rotational velocities of the active triangle which simplify to Eqs. (6) and (7) by fixing $\alpha_{12} = \alpha_{13} = 0$, $\alpha_{23} = \alpha$, and $\alpha_{12} = \mp 2\pi/3$, $\alpha_{23} = 0$, $\alpha_{13} = \pm 2\pi/3$, respectively.

B. Passive triangle in external force field

For the passive triangle in the external force field we can follow the same approach as described for the active triangle above. The sedimentation velocity of the passive triangle is given by

$$\mathbf{v}_e = \frac{1}{3} \sum_{i=1}^{3} \left(\mu \mathbf{f}_i(\mathbf{r}, t) + \sum_{j\neq i} \mathcal{G}_{ij} \cdot \mathbf{f}_j(\mathbf{r}, t) \right). \tag{39}$$

where $\mathbf{f}_i = \mathbf{f}_e + \sum_{j\neq i} \mathbf{f}_s^{ij}$ is the total force (external+spring) acting on the ith bead. We assume that the relative displacement of the beads is dependent on the triangle orientation (see Fig. 1) that is $\boldsymbol{\xi}_{ij}(\theta) = \sum_n [\mathbf{A}_n^{ij} \sin(n\theta) + \mathbf{B}_n^{ij} \cos(n\theta)]$ and solve Eq. (1) for $\mathbf{A}_n^{ij}$ and $\mathbf{B}_n^{ij}$ by expanding it in the form shown by Eq. (36). Please note that for the passive triangle in the external force field the active force term in Eq. (36) has to be replaced by the external force. Substitution of the values of coefficients $\mathbf{A}_n^{ij}$ and $\mathbf{B}_n^{ij}$ into Eq. (39) yields Eqs. (10) and (11). Similarly, the angular velocity of the passive triangle can be written as

$$\begin{aligned} \Omega_e &= \frac{1}{l^2} \sum_{i=1}^{3} (\mathbf{r}_i \times \dot{\mathbf{r}}_i) \\ &= \frac{\mu}{l^2} (\mathbf{r}_i \times \mathbf{f}_i) + \frac{1}{l^2} \sum_{i=1}^{3} (\mathbf{r}_i \times (\mathcal{G}_{ij} \cdot \mathbf{f}_j)) \end{aligned} \tag{40}$$

which simplifies to Eq. (7) for small deformation of the triangle.

C. Active triangle in external force field

Here too, we follow the same approach with the total force on each bead given by Eq. (8). It needs to be pointed out that due to its activity the deformation of active triangle depends on its orientation θ as well as on time t. Therefore, the relative displacement of the beads $\boldsymbol{\xi}_{ij}(\theta,t) = \sum_n [\mathbf{A}_n^{ij}(t)\sin(n\theta) + \mathbf{B}_n^{ij}(t)\cos(n\theta)]$ has the time dependent coefficients $\mathbf{A}_n^{ij}(t)$ and $\mathbf{B}_n^{ij}(t)$. Assuming $\mathbf{A}_n^{ij}(t) = \mathbf{P}_n^{ij}\sin(\omega t) + \mathbf{Q}_n^{ij}\cos(\omega t)$ and $\mathbf{B}_n^{ij}(t) = \mathbf{R}_n^{ij}\sin(\omega t) + \mathbf{S}_n^{ij}\cos(\omega t)$ one can linearize Eq. (1) following similar approach as for Eq. (36) to obtain the coefficients. Substitution of these coefficients in Eqs. (39) and (40) along with the appropriate values of phase angles α_{ij} gives us the desired analytical expressions.

[1] Eric Lauga and Thomas R Powers. The hydrodynamics of swimming microorganisms. *Reports on Progress in Physics*, 72(9):096601, 2009.

[2] N. P. Barry and M. S. Bretscher. Dictyostelium amoebae and neutrophils can swim. *Proc. Natl. Acad. Sci. U.S.A.*, 107(25):11376–11380, Jun 2010.

[3] Q. Wang and H. G. Othmer. Computational analysis of amoeboid swimming at low Reynolds number. *Journal of Mathematical Biology*, 72(7):1893–1926, 2016.

[4] A. Farutin, S. Rafai, D. K. Dysthe, A. Duperray, P. Peyla, and C. Misbah. Amoeboid swimming: a generic self-propulsion of cells in fluids by means of membrane deformations. *Phys. Rev. Lett.*, 111(22):228102, Nov 2013.

[5] A. Ghanbari, M. Bahrami, and M. R. H. Nobari. Methodology for artificial microswimming using magnetic actuation. *Physical Review E*, 83:046301, Apr 2011.

[6] Soichiro Tottori and Bradley J. Nelson. Artificial helical microswimmers with mastigoneme-inspired appendages. *Biomicrofluidics*, 7:061101, 2013.

[7] Ali Najafi and Ramin Golestanian. Simple swimmer at low reynolds number: Three linked spheres. *Physical Review E*, 69:062901, 2004.

[8] M. S. Rizvi, A. Farutin, and C. Misbah. Three-bead steering microswimmers. *Physical Review E*, 97(2):023102, Feb 2018.

[9] Patrick Degen. Self-propelling capsules as artificial microswimmers. *Current Opinion in Colloid and Interface Science*, 9:611–619, 2014.

[10] G. Lumay, N. Obara, F. Weyer, and N. Vandewalle. Self-assembled magnetocapillary swimmers. *Soft Matter*, 9:2420–2425, 2013.

[11] G. Grosjean, G. Lagubeau, A. Darras, M. Hubert, G. Lumay, and N. Vandewalle. Remote control of self-assembled microswimmers. *Nature Scientific Reports*, 5:16035, 2015.

[12] Stark H. Swimming in external fields. *The European Physical Journal Special Topics*, 225(11-12):2369–2387, 2016.

[13] D. P. Hader. Polarotaxis, gravitaxis and vertical phototaxis in the green flagellate, Euglena gracilis. *Arch. Microbiol.*, 147(2):179–183, Mar 1987.

[14] A. M. Roberts. Mechanisms of gravitaxis in Chlamydomonas. *Biol. Bull.*, 210(2):78–80, Apr 2006.

[15] A. M. Roberts. The mechanics of gravitaxis in Paramecium. *J. Exp. Biol.*, 213(Pt 24):4158–4162, Dec 2010.

[16] J. O. Kessler. Hydrodynamic focusing of motile algal cells . *Nature*, 313:218–220, 1985.

[17] D. P. Hader and R. Hemmersbach. Gravitaxis in Euglena. *Adv. Exp. Med. Biol.*, 979:237–266, 2017.

[18] R. Hemmersbach, D. Volkmann, and D. P. Hader. Graviorientation in protists and plants. *J. Plant Physiol.*, 154(1):1–15, Jan 1999.

[19] D.-P. Hader, M. Lebert, and R. Hemmersbach. *Gravity and the Behavior of Unicellular Organisms*. Cambridge University Press, 2005.

[20] B. ten Hagen, F. Kummel, R. Wittkowski, D. Takagi, H. Lowen, and C. Bechinger. Gravitaxis of asymmetric self-propelled colloidal particles. *Nat Commun*, 5:4829, Sep 2014.

[21] A. I. Campbell and S. J. Ebbens. Gravitaxis in spherical Janus swimming devices. *Langmuir*, 29(46):14066–14073, Nov 2013.

[22] J. T. Kuhr, J. Blaschke, F. Ruhle, and H. Stark. Collective sedimentation of squirmers under gravity. *Soft Matter*, 13(41):7548–7555, Oct 2017.

[23] F. Ruhle, J. Blaschke, J.-T. Kuhr, and H. Stark. Gravity-induced dynamics of a squirmer microswimmer in wall proximity. *New Journal of Physics*, 20(2):025003, 2018.

[24] M. S. Rizvi, A. Farutin, and C. Misbah. Size and shape affect swimming of a triangular bead-spring microswimmer. *Physical Review E*, 98(4):043104, Oct 2018.

[25] R. E. Caflisch. Periodic solutions for three sedimenting spheres. *The Physics of Fluids*, 31(11):3175, July 1988.

[26] M. L. Ekiel-Jezewskaa and B. U. Felderhof. Periodic sedimentation of three particles in periodic boundary conditions. *The Physics of Fluids*, 17(9):093102, Aug 2005.

[27] M. Bukowicki, M. Gruca, and M. Ekiel-Jezewska. Dynamics of elastic dumbbells sedimenting in a viscous fluid: Oscillations and hydrodynamic repulsion. *Journal of Fluid Mechanics*, 767:95–108, 2005.

[28] F. Candelier and B. Mehlig. Settling of an asymmetric dumbbell in a quiescent fluid. *Journal of Fluid Mechanics*, 802:174–185, 2016.

[29] L. M. Hocking. The behaviour of clusters of spheres falling in a viscous fluid Part 2. Slow motion theory. *Journal of Fluid*

Mechanics, 20:129–139, 1964.
[30] J. M. Crowley. Viscosity-induced instability of one-dimensional lattice of falling sphere. *Journal of Fluid Mechanics*, 45:151, 1971.
[31] Zhang Chao-Ying, Tan Hui-Li, Liu Mu-Ren, Kong Ling-Jiang, and Shi Juan. Lattice boltzmann simulation of sedimentation of a single elastic dumbbell in a newtonian fluid. *Communications in Theoretical Physics*, 42(4):605, 2004.
[32] Antonio Suma, Giuseppe Gonnella, Gianluca Laghezza, Antonio Lamura, Alessandro Mossa, and Leticia F. Cugliandolo. Dynamics of a homogeneous active dumbbell system. *Phys. Rev. E*, 90:052130, Nov 2014.
[33] Maria L Ekiel-Jezewska and Eligiusz Wajnryb. Hydrodynamic orienting of asymmetric microobjects under gravity. *Journal of Physics: Condensed Matter*, 21(20):204102, apr 2009.
[34] I. M Janosi, T. Tel, D. E. Wolf, and J.A.C. Gallas. Chaotic particle dynamics in viscous flows: The three-particle Stokeslet problem. *Phys Rev E Stat Nonlin Soft Matter Phys*, 56(3):2858–2868, Sep 1997.
[35] Jose Garcia De La Torre and Victor A. Bloomfield. Hydrodynamic properties of macromolecular complexes. i. translation. *Biopolymers*, 16(8):1747–1763, 1977.
[36] Knut Drescher, Raymond E. Goldstein, Nicolas Michel, Marco Polin, and Idan Tuval. Direct measurement of the flow field around swimming microorganisms. *Phys. Rev. Lett.*, 105:168101, Oct 2010.
[37] M. L. Ekiel-Jezewska and E. Wajnryb. Equilibria for the relative motion of three heavy spheres in Stokes fluid flow. *Phys Rev E Stat Nonlin Soft Matter Phys*, 73(4 Pt 2):046309, Apr 2006.
[38] T. Goldfriend, H. Diamant, and T. A. Witten. Screening, Hyperuniformity, and Instability in the Sedimentation of Irregular Objects. *Phys. Rev. Lett.*, 118(15):158005, Apr 2017.
[39] Lukas Holzer and Walter Zimmermann. Particles held by springs in a linear shear flow exhibit oscillatory motion. *Phys. Rev. E*, 73:060801, Jun 2006.
[40] M. Polin, I. Tuval, K. Drescher, J. P. Gollub, and R. E. Goldstein. Chlamydomonas swims with two "gears" in a eukaryotic version of run-and-tumble locomotion. *Science*, 325(5939):487–490, Jul 2009.
[41] Vladimir Pletser, Josef Winter, Fabienne Duclos, Thierry Bret-Dibat, Ulrike Friedrich, Jean-Francois Clervoy, Thierry Gharib, Frederic Gai, Olivier Minster, and Patrik Sundblad. The first joint european partial-g parabolic flight campaign at moon and mars gravity levels for science and exploration. *Microgravity Science and Technology*, 24(6):383–395, Dec 2012.
[42] M. Enculescu and H. Stark. Active colloidal suspensions exhibit polar order under gravity. *Phys. Rev. Lett.*, 107(5):058301, Jul 2011.
[43] F. Ginot, A. Solon, Y. Kafri, C. Ybert, J. Tailleur, and C. Cottin-Bizonne. Sedimentation of self-propelled Janus colloids: polarization and pressure. *New Journal of Physics*, 20:115001, 2018.